Bifurcations in elliptical, asymmetric non-neutral plasmas

J. Fajans,[a] E. Gilson, and E. Yu. Backhaus
Department of Physics, University of California, Berkeley, Berkeley, California 94720-7300

(Received 22 May 2000; accepted 15 June 2000)

A pure electron plasma held in a Malmberg–Penning trap deforms into an ellipse when subjected to a stationary, $l=2$ voltage perturbation on the trap wall. At first, the plasma's ellipticity is proportional to the strength of the perturbation, but once the perturbation increases beyond a critical value, the plasma equilibrium bifurcates into two stable off-axis equilibria and an unstable saddle. At the bifurcation point, the $l=1$ diocotron frequency dips to near zero. The diocotron orbits become very elliptical just below the bifurcation, and, after the bifurcation, split into three classes delimited by a separatrix: two classes surrounding the individual new equilibria, and one class surrounding both equilibria. The mode frequencies slow near the separatrix, and the trajectories themselves slow near the saddle at the origin. Interaction with the elliptical mode causes the diocotron mode to spontaneously and reversibly jump across the separatrix. © *2000 American Institute of Physics.* [S1070-664X(00)04010-6]

I. STATIONARY ELLIPTICAL PERTURBATIONS

Pure-electron plasmas form into circular cylinders when confined in Malmberg–Penning traps (see Fig. 1) with azimuthally symmetric trap walls. When azimuthal sectors on the wall are biased to make a $V\cos 2\theta$-like voltage perturbation, the plasma deforms into an elliptical cylinder like that shown in Fig. 2. Despite the lack of azimuthal symmetry,[1] the plasma is stable, stationary in the lab frame, and reasonably long-lived.[2] Curiously, *negative* voltages attract the *negatively* charged plasma, while *positive* voltages repel the plasma. Thus, in Fig. 2 the plasma is squeezed away from the $+17$ V applied to the left and right sectors.

Some years ago, we studied the effects of small voltage perturbations on the plasma shape.[3,4] Recently we extended these studies to strong perturbations and highly deformed plasmas.[5,6] For a $V\cos 2\theta$-like perturbation, we predicted that the plasma becomes increasingly elliptical as the perturbation V increases. When V exceeds a critical voltage, the system undergoes a classic pitchfork bifurcation, and the plasma moves off center to one of two new equilibria. As illustrated in Fig. 3, these predictions are born out experimentally.[7]

Trap construction asymmetries favor one of the postbifurcation equilibria over the other, but the effect of these asymmetries can be tuned out by applying a small voltage to the top or bottom sectors or by making the left and right sector voltages slightly different. Here we tune by applying a voltage $V_b=\beta V$ to the bottom sector. Typically the balance proportionality $|\beta|$ is less than 0.005. The tuning is quite sharp; changing β by less than 0.0015 will consistently send the plasma up or down. In Fig. 3, for example, changing β from -0.0027 to -0.0031 changed the selected equilibrium. Over the course of a few days, however, the equilibrium β can drift.

The plasma's center-of-charge is plotted as a function of the perturbation voltage in Fig. 4 and the plasma's ellipticity is plotted in Fig. 5. The theory curves in both graphs are derived from a second-moment Hamiltonian model given by Chu.[4,6] The model describes two-dimensional (2D) motion in the plane perpendicular to the trap axis (and magnetic field), and assumes that the plasma has a flat-top density n and an area A_p. Motion along the trap axis is ignored. Chu's Hamiltonian is the sum of three terms: H_s, the exact self-interaction energy of an elliptical plasma in free space; H_c, the exact interaction energy of a circular plasma with its own image and with the external potential $\phi(r,\theta)$; and H_λ, a series expansion, accurate to order A_p^3, of the interaction energy with the image and with the applied field due to the deviation of the plasma from circular to elliptical. Thus,

$$H_s=-\frac{V_p^2}{2}\ln\left[\frac{(1+\lambda)^2}{4\lambda}\right], \tag{1}$$

$$H_c=-V_p\phi(r,\theta)+V_p^2\ln\left(1-\frac{r^2}{R^2}\right), \tag{2}$$

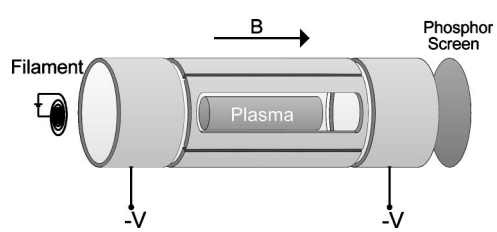

FIG. 1. Basic Malmberg–Penning trap geometry. Negatively biasing the end cylinders provides axial confinement, and the axial magnetic field provides radial confinement. The plasma is emitted from the filament on the left, and loaded into the trap by temporarily grounding the left cylinder. Details of the trap operation can be found in Ref. 14. The center section of the trap wall shows three of the four electrically isolated, azimuthal sectors, which, when biased appropriately, produce the desired $\cos 2\theta$-like voltage perturbation.

[a]Electronic mail: joel@physics.berkeley.edu

 © 2000 American Institute of Physics

Downloaded 20 Sep 2000 to 128.32.210.147.Redistribution subject to AIP copyright, see http://ojps.aip.org/pop/popcpyrts.html.

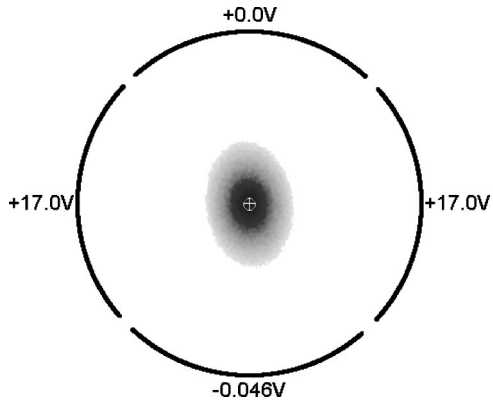

FIG. 2. Experimental image of the end view of a plasma deformed into an ellipse by the application of $+17.0$ V to the side sectors. The -0.046 V applied to the bottom sector is a balancing voltage, described later in the paper.

$$H_\lambda = \frac{V_p A_p}{8\pi}\left(\frac{1-\lambda^2}{\lambda}\right)\left[\frac{2V_p r^2}{(R^2-r^2)^2}\cos 2(\theta-\varphi) + \cos 2(\theta-\varphi)\frac{\partial^2\phi}{\partial^2 r} - \frac{\sin 2(\theta-\varphi)}{r}\frac{\partial^2\phi}{\partial r\partial\theta} + \frac{\sin 2(\theta-\varphi)}{r^2}\frac{\partial\phi}{\partial\theta}\right]. \tag{3}$$

To Chu's Hamiltonian we add a ''magnetron'' term coming from the confining fields at the ends of the trap,

$$H_m = -\frac{V_p r^2}{R^2}V_m - \frac{V_p A_p}{4\pi\lambda R^2}(1+\lambda^2)V_m. \tag{4}$$

Here r and θ are the position and angle of the center-of-charge of the plasma, λ is the aspect ratio of the plasma, and φ is the angle between the major axis of the plasma and the $\hat{x}$ axis. All the terms in the Hamiltonian are normalized by $4\pi\varepsilon_0$, and are in mks units. The plasma density n enters these equations through $V_p = enA_p/4\pi\varepsilon_0$, where e is the magnitude of the electron charge. The momenta conjugate to θ and φ are $P_\theta = (BV_p/2)r^2$ and $P_\varphi = (BV_pA_p/8\pi)[(1+\lambda^2)/\lambda]$, where B is the trap's axial magnetic field. As with the terms proportional to the external potential, the magnetron terms come from averaging the magnetron potential, $V_m r^2/R^2$ over the 2D elliptical plasma, where the proportionality V_m comes from averaging the confining field's radial component over the plasma length. The magnetron term adds an extra drive equal to $(2c/BR^2)V_m$ to both the $\dot{\theta}$ and the $\dot{\varphi}$ equations of motion.

II. BIFURCATIONS

If the external potential is given by $V\cos 2\theta$, $V_m = 0$, and, if corrections from $\lambda \neq 1$ are ignored, then the position of the plasma is given by

$$x = 0,$$

$$y = \begin{cases} 0 & V < V_c \\ R\sqrt{1 - V_c/V} & V > V_c \end{cases},$$

where the critical bifurcation voltage V_c equals V_p. In the experiment, however, the trap's four 90° sectors do not generate a pure $\cos 2\theta$ field; rather, they generate a field given by the Fourier sum $\phi(r,\theta) = V\Sigma A_m \cos m\theta$, where $A_m = (-1)^{[(m-2)/4]}(4/m\pi)$, $m = 2,6,10,\ldots$. Consequently the equilibrium must be found by solving for $\dot{r} = 0$, $\dot{\theta} = 0$, $\dot{\varphi} = 0$, and $\dot{\varphi} = 0$ numerically. Moreover, our plasma is neither

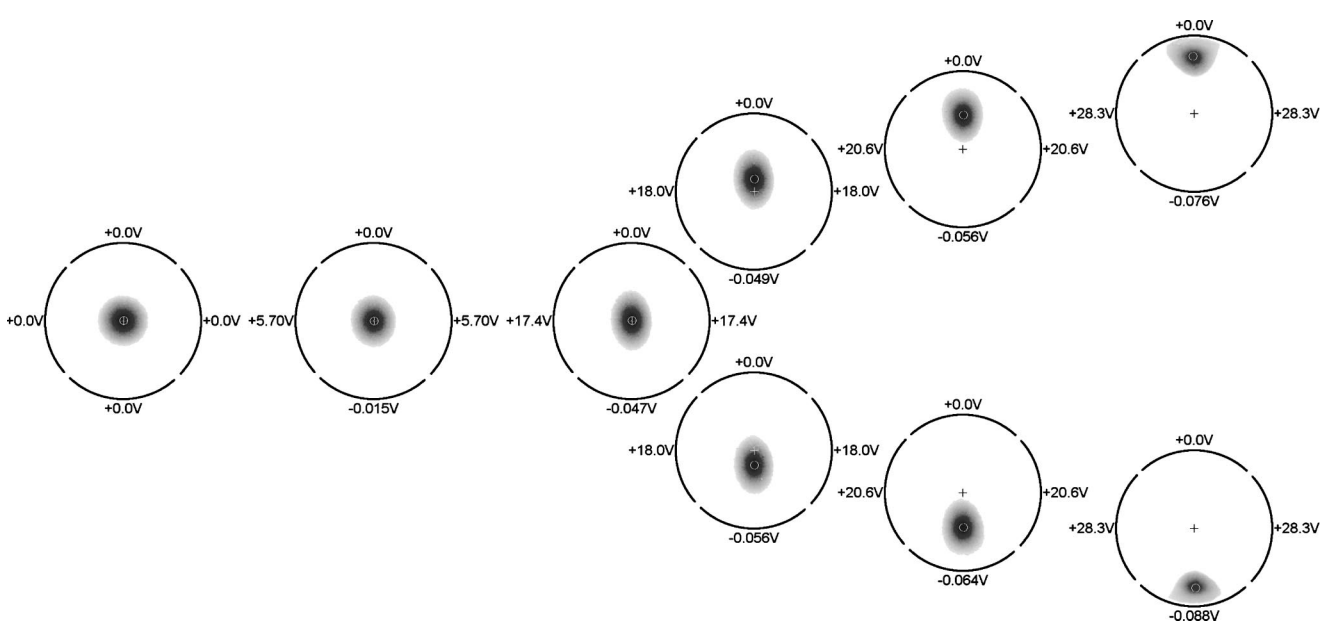

FIG. 3. Experimental images of the end view of a plasma as it is subjected to ever greater voltages on the side sectors. The bifurcation occurs at 17.67 V. The bottom sector is tuned to select the up or down equilibrium. In each image, the plus marks the center of the trap, while the small circle marks the center-of-charge of the plasma.

Downloaded 20 Sep 2000 to 128.32.210.147.Redistribution subject to AIP copyright, see http://ojps.aip.org/pop/popcpyrts.html.

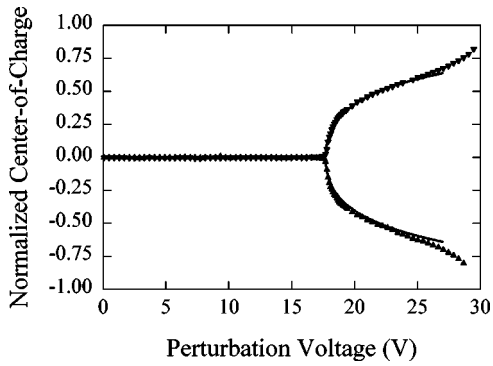

FIG. 4. Measured (triangles) and predicted (line) center-of-charge (normalized by the wall radius) of the ellipse as a function of the perturbation voltage. The bifurcation occurs at 17.67 V. The up and down equilibria are selected by tuning V_b.

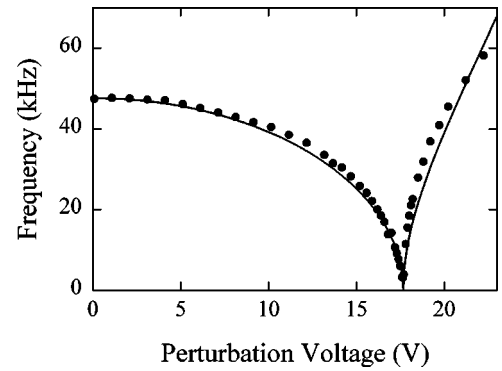

FIG. 6. Diocotron frequency as a function of the perturbation voltage. The measured values $f_0 = 47.6$ kHz and $V_c = 17.67$ V are used to calculate the theory line.

flat-topped nor infinite length, so we cannot use Chu's equations directly. In principle, we could find a new set of equations by averaging over the observed plasma density profile, and by bounce averaging along the trap axis. However, we can get satisfactory results simply by defining V_p such that the theory predicts the bifurcation to occur at the measured bifurcation voltage $V_c = 17.67$ V. Thus,

$$V_p = \frac{A_2 V_c - V_m}{1 - \frac{A_p}{4\pi R^2}\frac{\lambda_c^2 - 1}{\lambda_c}}, \tag{5}$$

where $A_2 V_c$ is the $\cos 2\theta$ component of the external potential at the bifurcation, and $\lambda_c = 1.45$ is the measured ellipticity at the bifurcation. The value of the magnetron potential, $V_m = 6.1$ V, is determined from the measured plasma density and confining fields.[8] Equation (5) depends weakly on the plasma area A_p, but Chu's A_p also assumes that the plasma is flat-topped. Fortunately, the initial slope of the V vs ellipticity data is proportional A_p, so we can find V_p and an effective A_p by using this slope and the measured bifurcation voltage simultaneously. The resulting theory lines are plotted in Figs. 4 and 5. The discrepancy between the ellipticity data and theory curve for very large voltages is probably due to the higher order terms in the potential. Such terms are increasingly important as the plasma approaches the wall, as is clearly visible for the $V = 28.3$ V plasmas in Fig. 3.

III. DIOCOTRON MODE

An important prediction of the theory is that the diocotron frequency goes to zero at the bifurcation. The $l = 1$ diocotron mode is driven by the plasma image charge fields, but, at the bifurcation, these fields are canceled by the fields from the perturbation voltage. Consequently the diocotron stalls. Theoretically, the small-amplitude diocotron frequency should be

$$f = \begin{cases} f_0\sqrt{1 - V/V_c} & V < V_c \\ 2\, f_0 (V/V_c)^{3/2}\sqrt{1 - V_c/V} & V > V_c \end{cases}, \tag{6}$$

where f_0 is the unperturbed diocotron frequency. As shown in Fig. 6, this prediction is verified by our experiments. However, the measured diocotron frequency does not go precisely to zero at the bifurcation. The minimum frequency is a sharp function of the balance proportionality (see Fig. 7). When detuned, nonlinearities dropped in the analysis leading to Eq. (6) keep the diocotron frequency finite. The importance of these nonlinearities is magnified by the shape of the diocotron orbits near the bifurcation, which, as shown in Fig. 8, becomes extremely elliptical. Even very low amplitude or-

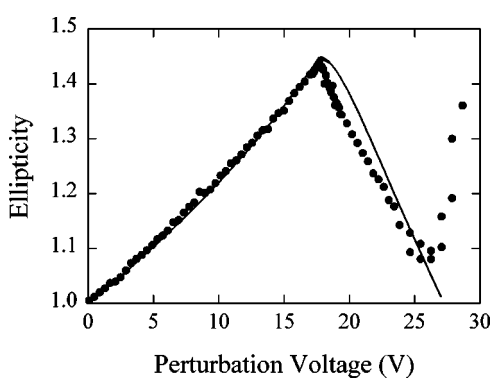

FIG. 5. Measured (dots) and predicted (line) ellipticity as a function of the perturbation voltage.

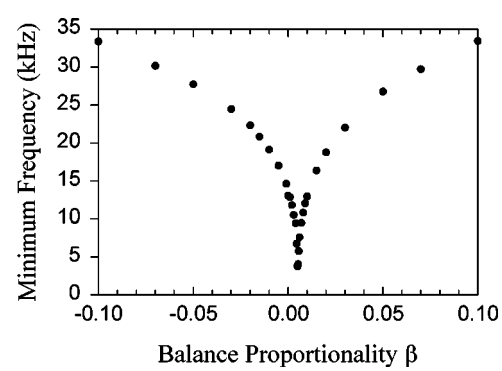

FIG. 7. Minimum diocotron frequency as a function of the balance proportionality β. (The optimal β, $+0.005$, has drifted from the optimal β found in Fig. 3.)

Downloaded 20 Sep 2000 to 128.32.210.147.Redistribution subject to AIP copyright, see http://ojps.aip.org/pop/popcpyrts.html.

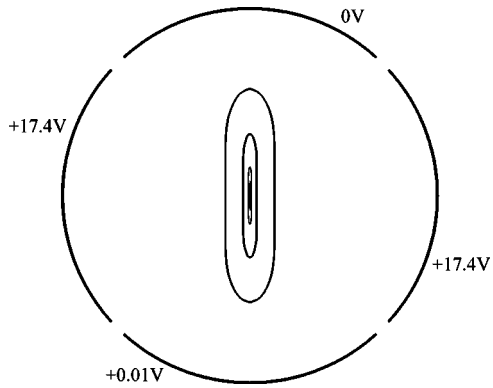

FIG. 8. Measured diocotron orbits just below bifurcation. Proceeding outwards, the orbit frequencies are 4, 8, 16, and 16 kHz. The ellipticity of the 4 kHz orbit is almost 28.

bits have large vertical excursions, and sample the nonlinearities found away from the origin. The postbifurcation diocotron orbits (Fig. 9) exhibit all the phase-space features associated with a 2D bifurcation;[9] there are teardrop shaped closed orbits around each of the two new equilibria as well as peanut shaped orbits which close around both equilibria, the equilibria themselves are separated by a saddle, the saddle connects to a separatrix which delimits the teardrop and peanut orbits, the orbit frequencies are lowest near the separatrix, and the orbital velocities slow near the saddle.

Classically, the separatrix between the teardrop and peanut orbit is inviolable. We find, however, that if we drive the diocotron mode too close to the separatrix, the plasma can spontaneously jump between the three orbit classes. The jumps are not repeatable, and occur at random intervals. A typical sequence is shown in Fig. 10. All the teardrop orbits in the sequence have roughly the same frequency, implying that the teardrop orbit amplitudes do not change. The peanut orbit frequencies are approximately half the teardrop orbit

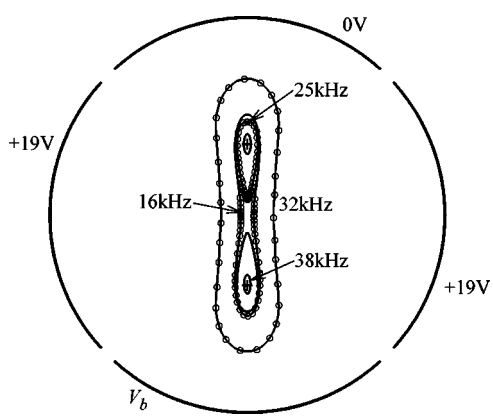

FIG. 9. Measured diocotron orbits above bifurcation showing teardrop shaped orbits surrounding one or the other of the two equilibria (marked by +'s), and peanut shaped orbits surrounding both equilibria. The signal on the bottom sector, V_b, is tuned to select the upper or lower equilibria. The origin is a saddle, and the separatrix is between the 25 kHz and 16 kHz orbits. Note how the orbital frequencies decrease near the separatrix. The circles denote 1 μs intervals along the orbit, and as expected the orbital velocity slows near the saddle at the origin. For clarity, the circles are suppressed on the upper half of the 16 kHz orbit, the lower 25 kHz orbit, and on both the 38 kHz orbits.

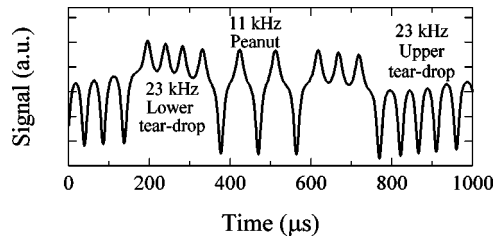

FIG. 10. Signal induced on the upper sector by the plasma charge demonstrating separatrix jumping. The magnitude and sign of the signal depends on the position of the plasma, with large negative-going signals indicating that the plasma is close to the upper sector, and smaller positive-going signals indicating that the plasma is far from the upper sector. The labels indicate the instantaneous orbit class.

frequencies. As the jumps can continue for over fifty milliseconds, making many transitions therein, they cannot be due to dissipation. We suspect that they are caused by an exchange of energy between the diocotron mode and the elliptical mode; strictly speaking, the separatrix only exists for the two-dimensional (x_c, y_c) system, not for the full $(x_c, y_c, \lambda, \varphi)$ system. Previous experiments on adiabatic invariants[10] two-vortex stability[11] and on autoresonance[12] have demonstrated that the diocotron mode is well decoupled from the elliptical mode. Effectively irreversible interactions[13] have been observed between the diocotron and elliptical modes, but this may be the first time that reversible coupling has been observed.

IV. CONCLUSIONS

Because of the close relationship between the equations describing the behavior of pure-electron plasmas and the behavior of two-dimensional, inviscid fluids, all of the phenomena reported here also occur in two-dimensional fluids. The plasma corresponds to a vortex; thus an external quadrupolar strain applied to a vortex will cause it to deform, and a strong enough strain will cause the vortex to bifurcate away from the center of the strain.

ACKNOWLEDGMENTS

We thank J.S. Wurtele for his help with this problem. This work was supported by the Office of Naval Research.

[1] T. M. O'Neil, Phys. Fluids **23**, 2216 (1980).
[2] J. Notte and J. Fajans, Phys. Plasmas **1**, 1123 (1994).
[3] J. Notte, A. J. Peurrung, J. Fajans, R. Chu, and J. Wurtele, Phys. Rev. Lett. **69**, 3056 (1992).
[4] R. Chu, J. S. Wurtele, J. Notte, A. J. Peurrung, and J. Fajans, Phys. Fluids B **5**, 2378 (1993).
[5] J. Fajans, E. Yu. Backhaus, and J. McCarthy, Phys. Plasmas **6**, 19 (1999).
[6] E. Yu. Backhaus, J. Fajans, and J. S. Wurtele, Phys. Plasmas **6**, 19 (1999).
[7] See EPAPS Document No. E-PHPAEN-7-040010 for a movie showing the bifurcation. This document may be retrieved via the EPAPS home page (http://www.aip.org/pubservs/epaps.html) or from ftp.aip.org in the directory/epaps/. See the EPAPS home page for more information.
[8] We need to calculate the length to find V_m. Rather than use a full numeric simulation, we use the simplification that the plasma ends where the vacuum fields equal half the plasma central potential. This simplification is based on calculations in A. J. Peurrung and J. Fajans, Phys. Fluids B **2**, 693 (1990), and has proved accurate in the past.
[9] See EPAPS Document No. E-PHPAEN-7-040010 for an animation of the

Downloaded 20 Sep 2000 to 128.32.210.147.Redistribution subject to AIP copyright, see http://ojps.aip.org/pop/popcpyrts.html.

post-critical diocotron orbits. This document may be retrieved via the EPAPS home page (http://www.aip.org/pubservs/epaps.html) or from ftp aip.org in the directory/epaps/.
[10]J. Notte, J. Fajans, R. Chu, and J. Wurtele, Phys. Rev. Lett. **70**, 3900 (1993).
[11]T. B. Mitchell, Ph.D. thesis, University of California, San Diego, 1993.
[12]J. Fajans, E. Gilson, and L. Friedland, Phys. Plasmas **6**, 4497 (1999).
[13]T. Mitchell and C. F. Driscoll, Phys. Fluids **8**, 1828 (1996).
[14]J. H. Malmberg, C. F. Driscoll, B. Beck, D. L. Eggleston, J. Fajans, K. Fine, X. P. Huang, and A. W. Hyatt, in *Non-Neutral Plasma Physics*, edited by C. Roberson and C. Driscoll (American Institute of Physics, New York, 1988), Vol. 175, p. 28.

Downloaded 20 Sep 2000 to 128.32.210.147.Redistribution subject to AIP copyright, see http://ojps.aip.org/pop/popcpyrts.html.